Mechanism and Kinetics of the Reaction of Acetylene and Nitric Oxide

Hue Minh Thi Nguyen,[†,‡] Raman Sumathi,[§] and Minh Tho Nguyen*[,†]

Department of Chemistry, University of Leuven, Celestijnenlaan 200F, B-3001 Leuven, Belgium, College of Education, Vietnam National University, Hanoi, Vietnam, and Lehrstuhl für Theoretische Chemie, Universität Bonn, Wegelerstrasse 12 D-53115, Bonn, Germany

Received: October 27, 1998; In Final Form: April 15, 1999

The potential energy surface (PES) of a [C_2,H_2,N,O] system in its electronic doublet ground state has been investigated using density functional theory method, at B3LYP/6-311++G(3df,2p)// B3LYP/6-311++G-(d,p) level. Twelve stable intermediate radicals including trans-nitrosoethenyl **1**, cis-nitrosoethenyl **2**, iminoketenyl **11**, and aminoketenyl **12** radicals have been located. Other stationary points on the PES formed from hydrogen migration and dissociation channels of these intermediates have been identified. Barrier heights, vibrational wavenumbers and moments of inertia were then utilized in the calculations of rate constants using quantum Rice−Ramsperger−Kassel (QRRK) theory. The total rate constant is found to increase with increase of temperature. At temperatures below 1000 K, only a rapid equilibrium is established between the reactants and the trans-nitrosoethenyl **1** radical which, in turn, suggests an absence of a reaction at low temperatures. HCO + HCN is found to be the predominant product at high temperatures and it involves five isomers of [C_2,H_2,N,O] system as intermediates with the formation of the four-membered ring **3** as the rate determining step. The rate constant for the formation of HCO + HNC is found to be 2 orders of magnitude lower than that for HCO + HCN. The total rate constant is pressure independent at low pressures up to atmospheric pressure. The calculated total rate constant at 2000 K and 1 atm pressure is 7.9×10^4 cm^3 mol^{-1} s^{-1}.

Introduction

The pyrolysis of acetylene has been extensively studied over the past sixty years. The salient aspects of the pyrolysis are (a) from 400 to 700 °C the reaction is an autocatalyzed radical chain polymerization[1−3] producing very few species smaller than C_4H_4; (b) the overall reaction rate is close to second order in acetylene concentration;[1−5] (c) there is a distinct and reproducible induction period which decreases with increasing temperature and increasing acetylene concentration;[1,2,5] (d) small amounts of NO (0.1−20%) inhibit the reaction;[1,2,6,7] (e) during the NO inhibited reaction, NO is very slowly consumed together with some acetylene after which the reaction proceeds at its normal rate;[1,2] (f) NO inhibits the gas-phase reaction[8] up to 1400 K, even at 2% NO concentration while above 2000 K, NO was found to have no effect on the pyrolysis of acetylene. Hence, the inhibiting effect by nitrogen oxide on the pyrolysis of aceylene is of great interest. However, only a few studies have been reported on the kinetics or the chemistry of the NO−C_2H_2 system which we explore here.

Frank-Kamenetsky[1] studied this reaction over the range 673−973 K. He reported that the rate of loss of NO (k_{NO}) during the induction period is very slow but is second order in C_2H_2 and virtually independent of NO concentration. On the basis of his experimental findings he proposed a kinetic scheme wherein NO disappears in a bimolecular reaction with a radical in the system which is produced during the bimolecular reactions of C_2H_2. More specifically, according to his scheme, NO radicals are not involved in the initiation step. The low-temperature studies (625−745 K) were made by Silcocks.[2] He reported a first-order dependence on C_2H_2 and a fractional order dependence (0.24) on NO for k_{NO}. The third study was the single pulse shock study by Ogura[8] at about 2.5 atm over the temperature range 1100−1650 K. This author found about a 1:1 production of CO and HCN which accounted for about 90% of the NO used. CO and HCN were formed at about 0.15 to 0.50 of the rate of formation of the major product, vinylacetylene, in the second-order process from C_2H_2 and NO. The radical chain mechanism was reported to be initiated by the bimolecular reaction of acetylene, viz.,

$$2C_2H_2 \rightarrow C_4H_3 + H$$

yielding 1-ethynyl and 2-ethynylvinyl radicals as the chain carriers. However, the experimental observations of Ogura led Benson[9] to suggest a radical chain mechanism as follows:

$$NO + C_2H_2 \xrightarrow{i} H + CO + HCN$$

$$H + C_2H_2 \overset{1}{\rightleftharpoons} C_2H_3(V^{\cdot})$$

$$V^{\cdot} + C_2H_2 \overset{2}{\rightleftharpoons} CH_2{=}CH{-}CH{=}CH^{\cdot} \overset{2H}{\rightleftharpoons} CH_2{=}CH{-}C{\equiv}CH$$

$$V^{\cdot} + NO \overset{t}{\rightleftharpoons} C_2H_3NO \rightarrow CH_2O + HCN$$

in which chains are both started and stopped by NO. The initiation step is not a simple bimolecular reaction and could proceed via one or more intermediates, and therefore it was difficult to select the rate determining step for the overall path.

In other words, the radical initiation step in the pyrolysis of acetylene is not yet known for certain. Also, the mechanism for the formation of CO in reactions of C_2H_2 + NO is not yet

* Corresponding author: e-mail, minh.nguyen@chem.kuleuven.ac.be.
† University of Leuven.
‡ Vietnam National University.
§ Universität Bonn.

10.1021/jp984243d CCC: $18.00
Published on Web 06/15/1999

SCHEME 1

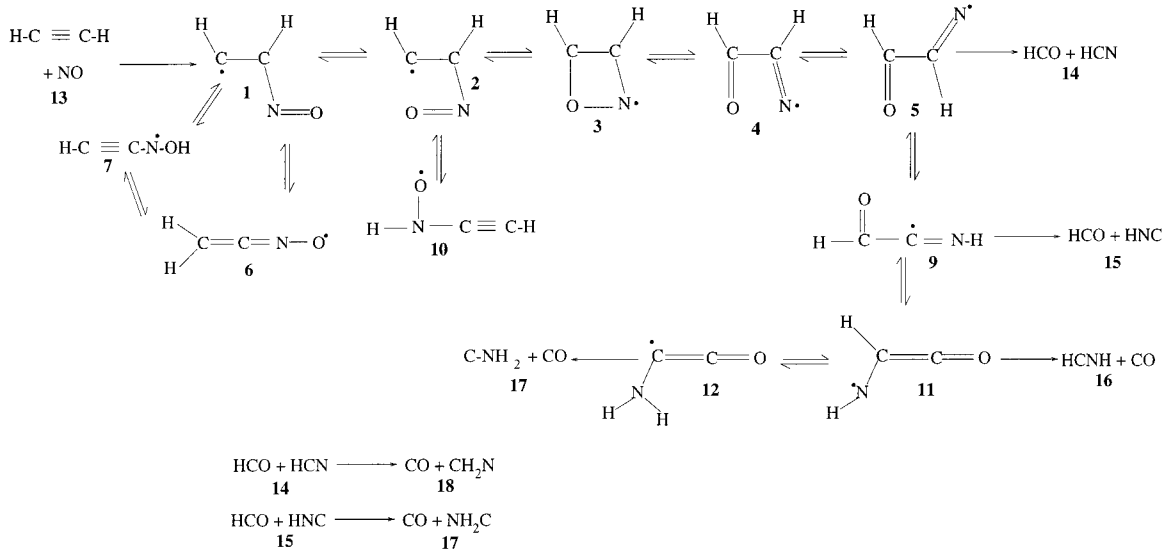

clear. Furthermore, in addition to H + CO + HCN, one can expect other products, viz., CO + HCNH, CO + H_2CN, CO + CNH_2, and HCO + HNC, in the reactions of acetylene with NO. Of the latter, CO + CH_2N and CO + HCNH are thermochemically more stable than HCO + HCN. To our knowledge, the existing theoretical work[10−14] on [C_2,H_2,N,O] is largely confined to the captodative and anomeric effects in the radical, CH(OH)CN. Hence, as a first step toward an understanding of the reaction mechanism, we wish to establish its potential energy surface (PES) as completely as possible. In this regard, we consider the possible isomerization and dissociation channels on the lowest-lying doublet state of [C_2,H_2,N,O] isomers. Since our interests are in characterizing all stationary points on the surface at a uniform and reliable level of treatment, we adopt here the computationally less demanding density functional approach. Furthermore, it has been shown very recently by Jursic[15a] that the best agreement with experimental geometries,[15b−g] enthalpies of formation,[15h−i] enthalpies of reaction, bond dissociation energies,[15j−o] and reaction barriers[15p−q] can be obtained with the hybrid B3LYP density functional method through an extensive exploration of the potential energy surface of HONO and other smaller polar nitrogen system by using a series of DFT and CBSQ methods. After mapping out the energy surface, we have utilized the computed thermochemical, vibrational, and rotational parameters of the stationary points as inputs for calculating the individual and total rate constants of C_2H_2 + NO reaction within the framework of the quantum Rice−Ramsperger−Kassel−Marcus (QRRK) theory.[16] The kinetic analysis allows the possibility of formation of each isomer and the competition between various reaction channels to be established. Despite being a less rigorous approach compared to the conventional Rice−Ramsperger−Kassel−Marcus (RRKM) theory, the overall reaction mechanism can be extracted from this simple treatment. The main advantage of the QRRK treatment lies in the fact that it is easy to implement for chemically activated reactions containing several energized intermediates and multiple channels. Our experience[17−28] shows that this approach wherein the ab initio structural and energetic parameters are combined with the QRRK formalism yields a very good picture about the reaction mechanism as well as the magnitude of the overall rate constants.

Method of Calculation

Ab initio molecular orbital calculations were carried out using the Gaussian 94 set of programs.[29] The open-shell calculations were performed using the unrestricted Hartree−Fock formalism. However, the major problem in the application of unrestricted spin formalism is that of contamination by higher spin states. It is thought that DFT methods using the unrestricted formalisms treat this in a better way than the molecular orbital UHF method does.[30] We initially optimized the geometries of reactants, adducts, and relevant transition structures with a 6-31G(d,p) basis set using the (U)B3LYP hybrid DFT method, in which the exchange functional consists of three terms, including the Hartree−Fock exchange functional.[31] The correlation functional is that of Lee, Yang, and Parr.[32] We performed an analytical vibrational frequency calculation in order to characterize the nature of the stationary points. The identity of each first-order stationary point is determined when necessary, by intrinsic reaction coordinate (IRC) calculations. Geometries were then reoptimized using the larger 6-311++G(d,p) basis set, and energies were computed at (U)B3LYP/6-311++G(3df,2p)//(U)-B3LYP/6-311++G(d,p) level and corrected subsequently for zero-point energies. Although the hybrid methods exhibit somewhat larger spin contamination than do the pure DFT methods owing to inclusion of the HF exchange,[30] the extent of contamination is sufficiently less than that for pure UHF wave functions.[33−35] As a measure of the spin contamination, we note that the expectation value of the $\langle S^2 \rangle$ operator was not greater than 0.76 for doublets. In general, the hybrid B3LYP functional with a large basis set is accurate for the computed structural parameters of small polar molecular systems.[15b−g] The computed geometries differ by less than 1% from the experimental values. This deviation is usually in the margins of the experimental error. The hybrid B3LYP method computed bond dissociation energies differ by approximately 1 kcal/mol from those calculated from the Complete Basis Set approach.[15a] DFT calculations have also been found[36] to yield realistic results for the prediction of transition states' geometries and energies. In the HONO system, the B3LYP/6-311G(3df,3pd) predicted barrier heights differ by less than 1 kcal/mol from those of the CBSQ computed values.[15a]

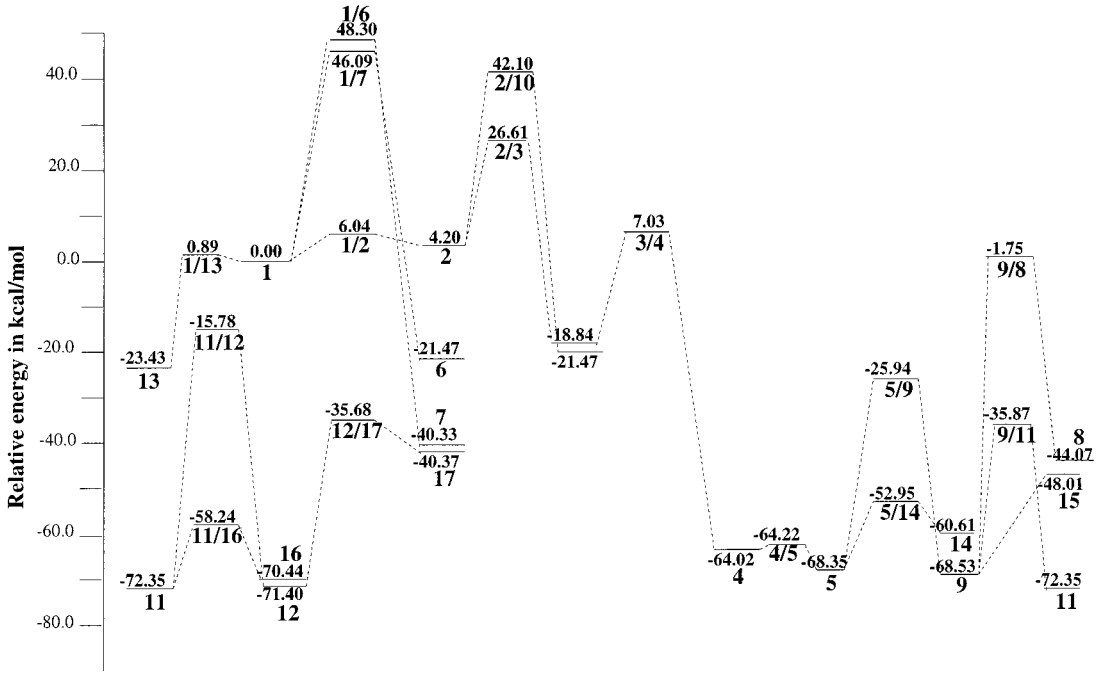

Figure 1. The overall profile of the doublet PES for the $[C_2,H_2,N,O]$ system calculated at the B3LYP/6-311++G(3df,2p)//B3LYP/6-311++G-(d,p)+ZPE level of theory.

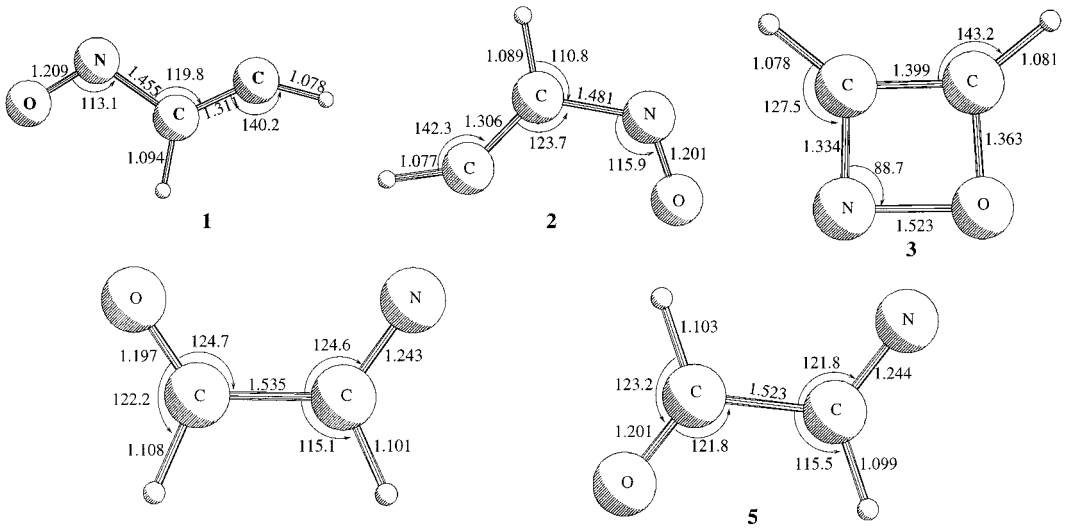

Figure 2. B3LYP/6-311++G(d,p) optimized geometries of the intermediates **1**, **2**, **3**, **4**, and **5** in the channel leading to HCO + HCN product.

Results and Discussion

The reactions investigated in this study are shown in Scheme 1. A schematic representation of the PES for the C_2H_2 + NO reaction is presented in Figure 1. Each stationary point in Figure 1 and Scheme 1 is labeled with a number in order to facilitate the discussion. While the various isomers of the $[C_2,H_2,N,O]$ system are associated with numbers from **1** to **12**, the various product limits, viz., HC≡CH + NO, HCO + HCN, HCO + HNC, CO + HCNH, CO + CNH_2, CO + CH_2 N are labeled, respectively, from **13** to **18**. The equilibrium geometries of the various $[C_2,H_2,N,O]$ isomers are presented in Figures 2 and 3. Figure 4 displays the B3LYP optimized transition state structures on the C_2H_2 + NO PES leading to HCO + HCN product. Figure 5 shows the various hydrogen migration transition states leading to other isomers of the $[C_2,H_2,N,O]$ system. The transition states for dissociation are presented in Figure 6 along with the direct hydrogen abstraction transition structures. In Figures 2−6, bond lengths are given in angströms and bond angles in degrees. In general, **X/Y** stands for a transition structure connecting the equilibrium structures **X** and **Y**. The magnitude of the barrier heights are tabulated in Table 1. The harmonic vibrational frequencies of the various $[C_2,H_2,N,O]$ isomers and transition structures for isomerization and dissociation are given, respectively, in Tables 2−4 along with the $\langle S^2 \rangle$ values.

The addition of NO radical to the stable acetylene molecule proceeds with a barrier of 24.3 kcal/mol and leads to a planar trans-nitrosoethenyl, HC=CH(NO) **1** (ONCC = 180°) radical. The reaction is endothermic by 23.4 kcal/mol. The existence of the entrance channel barrier and the fact that the adduct **1** is thermochemically less stable than the isolated reactants suggest this reaction to be unimportant at ordinary temperatures. Furthermore, the adduct is stabilized by a very shallow potential well. Owing to its very low barrier (0.9 kcal/mol) for dissociation, at ordinary temperatures, the rate of redissociation will be appreciable. In other words, there should be a rapid equilibrium between the reactants and the trans-nitrosoethenyl radical adduct,

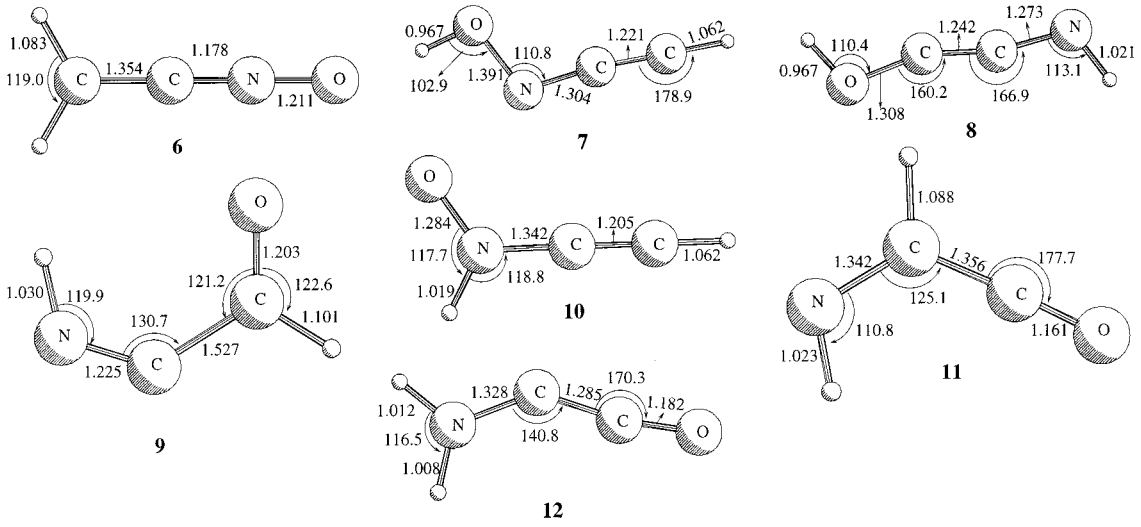

Figure 3. B3LYP/6-311++G(d,p) optimized geometries of the stationary points **6**, **7**, **8**, **9**, **10**, **11**, and **12** on the [C_2,H_2,N,O] system.

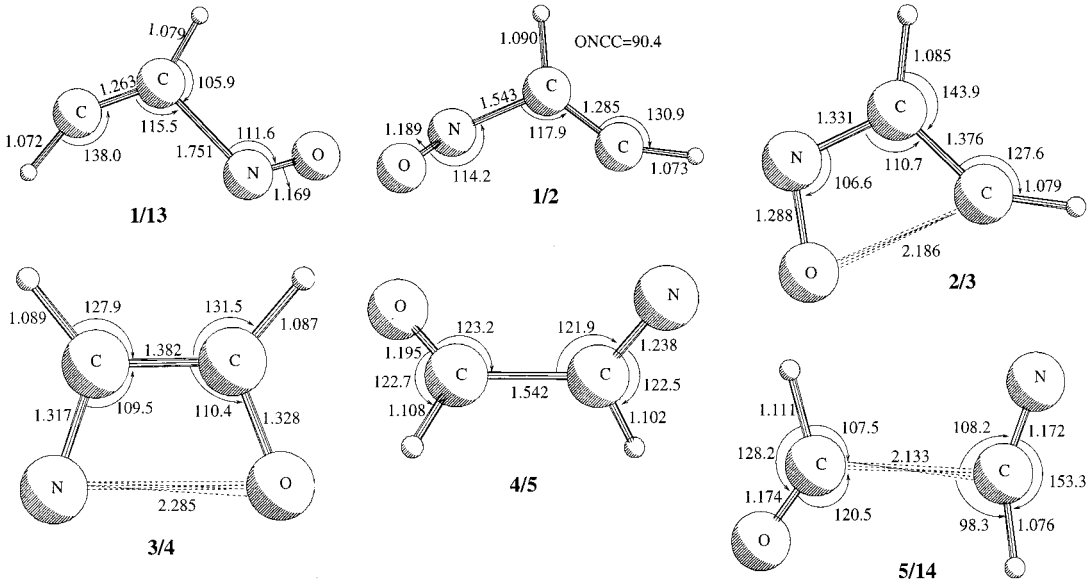

Figure 4. B3LYP/6-311++G(d,p) optimized geometries of the transition structures **1/13**, **1/2**, **2/3**, **3/4**, **4/5**, and **5/14** in the path leading to HCO + HCN product.

1. Moreover, the higher entropy of the reactants over that of the adduct helps shift the equilibrium away from the adduct, and hence no reaction between C_2H_2 and NO. Only at high-temperature pyrolyses can this reaction proceed forward forming other radical products.

The optimized geometry of radical **1** is shown in Figure 2, and the radical center is situated on the carbon atom. The radical adduct **1** thus formed can undergo either a cis−trans isomerization or hydrogen shifts, viz., 1,2- and 1,3- migrations. Although the products of hydrogen migration, **6** and **7**, are thermochemically more stable than **1**, their formation is kinetically unfavorable because of the existence of very large barriers (48.3 and 46.1 kcal/mol, respectively). The radical **1** will thus undergo cis−trans isomerization in addition to its redissociation at high temperatures. The cis isomer can then cyclize to form the four-membered ring **3** with the radical center on nitrogen. The cyclic isomer is energetically more stable compared to nitrosoethene radicals. However, it is strained because of the presence of a double bond within a four-membered ring and can undergo a spontaneous ring opening via the cleavage of the N−O bond, giving rise to the more stable HC(═O)−CH-(═N) **4** radical, and the transition structure for this process **3/4** as shown in Figure 1 lies below **2/3**. When formed from activated **1**, isomer **3** will be likewise energetically excited and so should rapidly dissociate to **4**. The optimized structure of **4** is also shown in Figure 2. The radical center is on the more electronegative nitrogen atom and it lies energetically below the starting reactants. Structurally **3/4** is very similar to **3**, as expected for such a highly exoergic process ($\Delta H = -45.4$ kcal/mol). This radical would then undergo an energetically feasible cis−trans isomerization and C−C bond cleavage giving rise to HCO + HCN **14**. Since HCO + HCN is formed from the energized radical **1**, it will have a minimum excess energy of 87.2 kcal/mol, and this excess energy will be distributed as translational, rotational, and internal energies of the products. This excess energy will result in the further cleavage of the C−H bond in the HCO radical as it involves a dissociation energy of only 21.0 kcal/mol at the same level of calculation.

In addition to dissociation, **5** can undergo a 1,2-hydrogen shift giving rise to an equally stable ketoiminyl radical **9**. However, the barrier for this migration is higher than that for the C−C bond dissociation. Furthermore, the dissociation transition state **5/14** is very loose with a long C−C bond (2.133 Å) compared to the isomerization transition state **5/9**. Hence, the magnitude

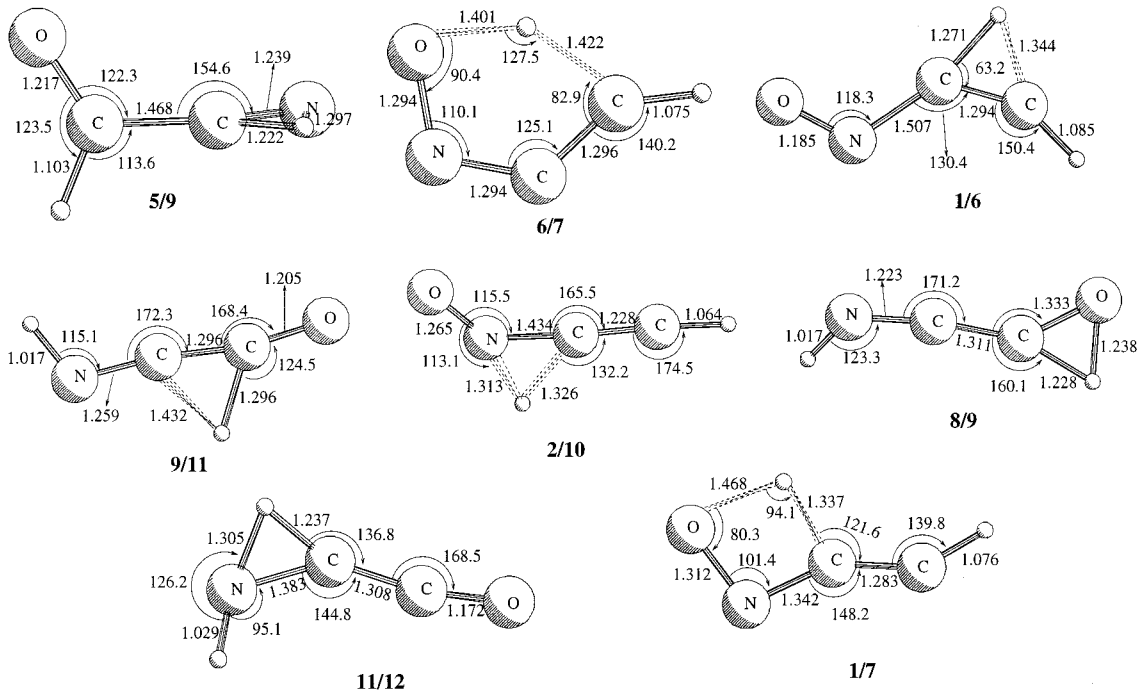

Figure 5. B3LYP/6-311++G(d,p) optimized geometries of the hydrogen migration transition structures **5/9**, **6/7**, **1/6**, **9/11**, **2/10**, **9/8**, **11/12**, and **1/7** on the $[C_2,H_2,N,O]$ PES.

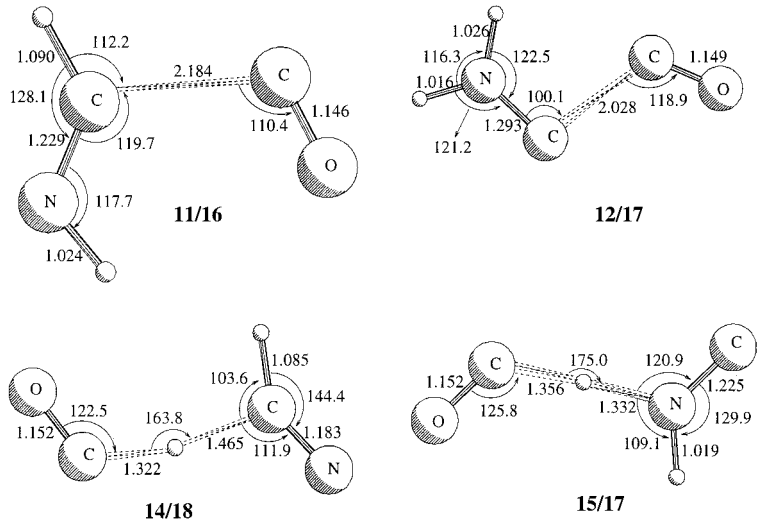

Figure 6. B3LYP/6-311++G(d,p) optimized geometries of the dissociation transition structures **11/16** and **12/17** and the direct hydrogen abstraction transition structures **14/18** and **15/17** on the $[C_2,H_2,N,O]$ PES.

of the preexponential factor for dissociation will be higher than that for the isomerization. The calculated preexponential factors for both the processes are 3.0×10^{12} and 1.92×10^{13} s^{-1}, respectively. Preexponential factors were calculated as

$$A_i = \frac{k_B T}{h} \frac{Q^{\dagger}}{Q}$$

where k_B is the Boltzmann constant, h Planck's constant, T the temperature in Kelvin, and $Q_i^{\dagger}$ and Q_i are the complete partition functions for the respective transition state and the reactant. The partition functions were obtained from the calculated harmonic vibrational frequencies and moments of inertia. These results indicate a competitive formation of **9** and HCO + HCN; however, with a greater preference for the latter. The isomer **9** thus formed will have more energy than the barrier for its dissociation (since **9/15** lies below **5/9**), and hence will spontaneously dissociate into HCO + HNC **15**. The most stable isomer of the $[C_2,H_2,N,O]$ system is the substituted ketene radical, O=C=CH−NH **11** which can exist in two resonance structures with the radical center either on a carbon or on a nitrogen atom.

$$O{=}\dot{C}{-}CH{=}NH(A) \leftrightarrow O{=}C{=}CH{-}\dot{N}H(B)$$

The optimized structure shown in Figure 3 suggests a predominant contribution from the resonance structure (B) with a carbon−carbon double bond (1.356 Å). As discussed above, the formation of isomer **9** itself is less favored, and once formed **9** would undergo a facile dissociation to HCO + HNC. Hence, the probability for the formation of **11** is still less compared to that of **9**. As such, the probability for a particular product formation decreases with increasing number of intermediates and it decreases still further when the energetics are unfavorable. The calculated preexponential factors for dissociation (to **15**) and isomerization (to **11**) from **9** at 300 K are 9.75×10^{14} and

TABLE 1: Zero-Point Energy Corrected Barrier Heights, E_a, and Heat of the Reaction, ΔE, in kcal/mol for the Various Reaction Channels on the [C_2,H_2,N,O] System

reaction	E_a	ΔE
1 → **2**	6.0	4.2
1 → **6**	48.3	−40.3
1 → **7**	46.1	−21.5
1 → **13**	0.9	−23.4
2 → **3**	22.4	−23.0
2 → **10**	37.9	−24.6
3 → **4**	25.9	−45.4
4 → **5**	0.2	−4.1
5 → **9**	42.4	−0.2
5 → **14**	15.4	7.7
6 → **7**	74.6	18.9
8 → **9**	42.3	−24.5
9 → **11**	32.7	−3.8
9 → **15**	20.5	20.0
11 → **12**	56.7	1.0
11 → **16**	14.1	1.9
12 → **17**	35.7	31.0
14 → **18**	13.0	−9.8

4.38×10^{12} s^{-1}, respectively. Thus the A factor is two orders of magnitude lower than that for dissociation. The present PES thus suggests HCO + HCN to be the major product of the C_2H_2 + NO reaction at higher temperatures in line with the experimental observations of Ogura.[8]

As can be seen from Figure 1, the step **2** → **3** is the rate determining step in the formation of CO. Once the cyclic isomer **3** is formed, it can undergo further isomerizations leading to thermochemically more stable isomers of [C_2,H_2,N,O] and the barriers for such isomerization are lower than the energy of the transition state **2/3**. In other words, initial reactants must acquire an energy equal to or greater than that of **2/3** in order to be the radical initiation step in acetylene pyrolysis. The present PES establishes the following pathways (A, B, C, and D) for the formation of CO with the rate determining **2** → **3** isomerization step

$$\mathrm{HC{\equiv}CH + NO} \xrightarrow{1/13} \mathbf{1} \xrightarrow{1/2} \mathbf{2} \xrightarrow{2/3} \mathbf{3} \xrightarrow{3/4} \mathbf{4} \xrightarrow{4/5} \mathbf{5} \xrightarrow{5/14} \mathbf{14}\ \text{Route(A)}$$

$$\mathrm{HC{\equiv}CH + NO} \xrightarrow{1/13} \mathbf{1} \xrightarrow{1/2} \mathbf{2} \xrightarrow{2/3} \mathbf{3} \xrightarrow{3/4} \mathbf{4} \xrightarrow{4/5} \mathbf{5} \xrightarrow{5/9} \mathbf{9} \xrightarrow{9/15} \mathbf{15}\ \text{Route(B)}$$

$$\mathrm{HC{\equiv}CH + NO} \xrightarrow{1/13} \mathbf{1} \xrightarrow{1/2} \mathbf{2} \xrightarrow{2/3} \mathbf{3} \xrightarrow{3/4} \mathbf{4} \xrightarrow{4/5} \mathbf{5} \xrightarrow{5/9} \mathbf{9} \xrightarrow{9/11} \mathbf{11} \xrightarrow{11/16} \mathbf{16}\ \text{Route(C)}$$

$$\mathrm{HC{\equiv}CH + NO} \xrightarrow{1/13} \mathbf{1} \xrightarrow{1/2} \mathbf{2} \xrightarrow{2/3} \mathbf{3} \xrightarrow{3/4} \mathbf{4} \xrightarrow{4/5} \mathbf{5} \xrightarrow{5/9} \mathbf{9} \xrightarrow{9/11} \mathbf{11} \xrightarrow{11/12} \mathbf{12} \xrightarrow{12/17} \mathbf{17}\ \text{Route(D)}$$

Since the dissociation transition structures are disposed energetically lower than the isomerization transition states from isomers **5**, **9**, **11**, and **12**, the dominant product is dictated to be HCO + HCN via Route A.

In addition to these channels, we have also investigated the direct hydrogen abstraction channels

$$\mathrm{HCO + HCN}\ \mathbf{14} \rightarrow \mathrm{CO + H_2CN}\ \mathbf{18}\ \text{(E)}$$

$$\mathrm{HCO + HNC}\ \mathbf{15} \rightarrow \mathrm{CO + H_2NC}\ \mathbf{17}\ \text{(F)}$$

The channel (E) is exothermic by 9.8 kcal/mol while channel (F) is nearly thermoneutral ($\Delta H = 0.7$ kcal/mol). The transition structures for both of the processes **14/18** and **15/17** are shown in Figure 6. As can be seen from Figure 1, the barrier heights for channel (E) and (F) are, respectively, 13.3 and 12.9 kcal/mol. The barrier heights are higher than the respective barriers for the formation of **5** (7.7 kcal/mol) from **14** and **9** from **15**. Hence, the reaction kinetics of HCO + HCN and HCO + HNC will proceed via the radical addition and will lead to the predominant formation of HC(O)CH(N) radical. We attempted to obtain the transition structures for the 1,1- elimination of CH_2N from radicals **4** and **5**, however, without much success. The direct hydrogen abstraction channel will contribute to the total rate of disappearance of the reactants only at high temperatures. The direct hydrogen abstraction rate constant has been calculated using the Arrhenius expression, $k = A \exp(-E_a/RT)$ where the preexponential factor A has been obtained from the partition function of the reactants and transition structure. The calculated rate constant at 300 K for channel (i) is 1.48×10^2 cm^3 mol^{-1} s^{-1}.

Kinetic Analysis of the C_2H_2 + NO Reaction. In an attempt to extract a finer mechanism of product formation, a kinetic analysis of C_2H_2 + NO reaction associated with the [C_2,H_2,N,O] PES has been performed. The apparent rate constants for the various product formations have been computed using the QRRK model. Recent publications[17−28,37] reveal that processes involving high energy chemically activated adducts with non-Boltzmann distribution can be characterized by the simple QRRK method with reasonable accuracy. In essence, quantum Kassel theory employs statistical mechanics to calculate the probability that sufficient energy will be localized in a given oscillator for the reaction to occur. Weston[38] has calculated the rate constants for nine reactions (viz., *n*-C_4H_{10} → $2C_2H_5$, C_2H_6 → $2CH_3$, PhCO → Ph + CO, CH_3 $NHNH_2$ → NH_3 + CH_2 ═NH, t-BuO → $(CH_3)_2$ CO + CH_3, CH_3 CO → CH_3 + CO, *n*-hexyl → *s*-hexyl, cyclobutene → butadiene, *cis*-butene-2 → *trans*-butene-2) using a wide range of temperatures and pressures and has shown that the quantum Kassel expression using the geometric mean of the molecular vibration frequencies provides better results than that using the arithmetic mean. He has also found that the QRRK values are in generally good agreement with RRKM values, and they also exhibit the monotonic decrease in k_0/k_∞ with increasing temperature that is characteristic of the RRKM results. A comparison of the reduced state density, $\rho(E)/Q$, as calculated by the Whitten−Rabinovitch method and the quantum Kassel methods has also been made by Weston. It has been shown that the energy dependence of ρ(E) is very nearly the same in both the approaches. Since the quantum Kassel expression uses a single-frequency model, one might anticipate that molecules with a widespread frequency distribution would cause problems. However, there seems to be no observable correlation with the frequency dispersion.[38] Since our interest is to obtain the finer details of the reaction mechanism rather than an accurate evaluation of the rate constant, we adopt here the reliable and less rigorous QRRK approach over the conventional RRKM treatment. Note that no experimental rate constant measurements are available for comparison. The kinetic treatment and the method of evaluation of the apparent rate constants for the stabilization of adducts and for the dissociation into products are well described in our previous papers.[17−28] For the description of collisional stabilization, we adopted the weak-collision model suggested by Troe,[39,40] and the collision rate is considered to be a product of the Lennard−Jones collision frequency, Z_{LJ} and collision efficiency, β. The collision efficiency, β was calculated from[40]

$$\frac{\beta}{(1-\beta^{1/2})} = -\langle \Delta E \rangle / F_E k_B T$$

TABLE 2: Unscaled B3LYP/6-31G(d,p) Harmonic Vibrational Frequencies of the Various Isomers on the PES of the (C_2,H_2,N,O) System

species	frequencies (cm^{-1})	ZPE (kcal/mol)	$\langle S^2 \rangle$
1	166.6, 364.7, 590.7, 676.6, 702.9, 844.9, 1015.5, 1215.2, 1549.7, 1670.9, 3079.4, 3288.9	21.7	0.75
2	136.3, 308.4, 556.3, 699.0, 824.8, 876.9, 930.8, 1230.4, 1520.5, 1709.6, 3125.1, 3285.9	21.7	0.75
3	439.2, 632.0, 667.5, 777.5, 923.1, 1018.9, 1043.2, 1277.6, 1358.4, 1447.2, 3237.3, 3282.1	23.0	0.752
4	90.4, 284.6, 704.2, 709.7, 852.8, 1019.4, 1202.3, 1411.6, 1683.9, 1845.6, 2928.8, 3001.5	22.5	0.75
5	145.7, 344.6, 535.1, 767.2, 972.4, 1010.0, 1174.1, 1394.0, 1700.8, 1817.6, 2994.1, 3034.2	22.7	0.75
6	190.5, 245.2, 351.3, 433.7, 667.8, 920.1, 1018.1, 1425.7, 1506.9, 2316.8, 3161.9, 3258.2	22.1	0.75
7	239.1, 386.4, 448.7, 528.5, 573.6, 645.0, 961.9, 1120.5, 1436.6, 2027.0, 3489.0, 3771.9	22.3	0.76
8	171.1, 177.6, 388.2, 389.4, 485.9, 889.4, 1081.2, 1257.1, 1500.8, 2132.2, 3467.4, 3740.6	22.4	0.752
9	192.1, 204.7, 615.9, 670.5, 871.6, 918.9, 992.4, 1380.8, 1526.4, 2071.6, 2986.6, 3422.3	22.7	0.751
10	227.2, 375.9, 449.3, 499.3, 630.7, 689.0, 1040.3, 1361.2, 1502.1, 2198.3, 3450.9, 3495.3	22.7	0.75
11	207.5, 282.1, 571.2, 678.5, 886.4, 1021.1, 1173.6, 1308.1, 1407.6, 2172.2, 3154.9, 3435.0	23.3	0.75
12	209.9, 336.2, 349.6, 491.0, 537.0, 951.6, 1147.2, 1598.7, 1671.7, 2202.5, 3535.9, 3660.0	23.9	0.75

TABLE 3: Unscaled B3LYP/6-31G(d,p) Harmonic Vibrational Frequencies of the Various Isomerization Saddle Points on the PES of the (C_2,H_2,N,O) System

species	frequencies (cm^{-1})	ZPE (kcal/mol)	$\langle S^2 \rangle$
1/2	204.1i, 317.1, 442.1, 516.6, 717.7, 752.5, 858.3, 1155.5, 1615.7, 1711.5, 3197.9, 3303.2	20.9	0.753
2/3	505.3i, 462.2, 780.9, 810.9, 848.6, 943.5, 1051.8, 1207.6, 1293.7, 1355.9, 3193.8, 3259.9	21.7	0.761
3/4	290.6i, 438.8, 674.0, 723.6, 798.9, 1039.8, 1118.9, 1221.7, 1373.9, 1473.1, 3135.9, 3168.6	21.7	0.754
4/5	167.5i, 298.0, 441.5, 750.6, 906.4, 985.9, 1181.6, 1391.1, 1717.9, 1843.2, 2934.4, 2981.4	22.1	0.75
1/6	2075.8i, 106.3, 288.6, 465.5, 479.3, 683.9, 815.5, 1412.2, 1668.4, 1753.8, 2323.6, 3158.4	18.8	0.754
1/7	2950.5i, 171.8, 270.0, 672.2, 688.4, 755.6, 1007.9, 1064.8, 1178.2, 1703.8, 1789.5, 3294.7	18.0	0.752
5/9	2019.1i, 166.9, 260.3, 299.6, 596.1, 845.2, 930.4, 1383.6, 1676.5, 1848.9, 2553.9, 2978.1	19.3	0.75
9/11	990.3i, 167.6, 264.8, 356.8, 462.6, 916.3, 960.7, 1039.0, 1622.4, 1985.0, 2238.2, 3536.1	19.4	0.75
2/10	1815.5i, 175.3, 335.8, 388.1, 547.2, 606.5, 673.7, 759.4, 1269.1, 1792.9, 2036.2, 3472.1	17.2	0.75
9/8	2041.8i, 200.9, 272.4, 349.3, 480.7, 648.6, 838.0, 932.3, 1427.3, 2028.9, 2602.5, 3486.2	18.9	0.75
11/12	1941.2i, 221.6, 305.4, 480.9, 600.6, 793.0, 912.4, 1222.1, 1441.8, 2157.3, 2451.2, 3321.9	19.9	0.75

TABLE 4: Unscaled B3LYP/6-31G(d,p) Harmonic Vibrational Frequencies of the Various Dissociation Saddle Points on the PES of the (C_2,H_2,N,O) System

species	frequencies (cm^{-1})	ZPE (kcal/mol)	$\langle S^2 \rangle$
1/13	598.5i, 88.0, 320.5, 443.8, 587.4, 666.9, 810.7, 1014.8, 1703.3, 1775.4, 3267.1, 3379.5	20.1	0.753
5/14	424.8i, 41.9, 209.0, 272.9, 559.1, 744.2, 828.3, 1136.3, 1919.2, 2019.8, 2840.3, 3341.8	19.9	0.75
9/15	306.4i, 52.8, 148.9, 258.8, 276.7, 402.9, 509.2, 1134.0, 1938.1, 1986.7, 2689.1, 3779.7	18.5	0.753
11/16	215.8i, 94.6, 130.5, 304.4, 370.8, 958.4, 1004.7, 1190.4, 1803.6, 2063.5, 3111.5, 3408.9	20.6	0.75
12/17	290.7i, 104.8, 267.0, 421.1, 519.6, 778.7, 1069.2, 1444.8, 1623.2, 2029.8, 3348.3, 3515.6	21.6	0.75
14/18	1702.5i, 62.9, 103.5, 252.2, 525.1, 549.1, 881.2, 1032.4, 1289.9, 1989.5, 2037.0, 3205.6	17.1	0.753
15/17	1892.2i, 62.6, 100.3, 265.7, 445.1, 537.0, 886.0, 974.2, 1415.9, 1790.2, 2025.2, 3482.1	17.1	0.75

The value of F_E was assumed to be 1.15 and the average energy transferred per collision was taken as 1.075 kcal/mol for N_2 as bath gas following the reference of Troe et al.[40] As suggested by Radom et al.,[41] a scaling factor of 0.9614 has been used to scale the harmonic vibrational frequencies in our kinetic calculations.

As discussed above, the C_2H_2 + NO reaction can give rise to **1** via the transition structure **1/13** at high temperatures. For this reaction, we calculated the apparent rate constants for the formation of various isomers and products (as shown in Figure 1) from C_2H_2 + NO. The apparent rate constants are labeled as k_n (n runs from 1 to 18 except 13) where n represents the product number as shown in Figure 1. The total rate constant, k_T for the disappearance of the C_2H_2 + NO reactants was calculated as the sum of all apparent rate constants. Figure 7 shows the variation of the apparent rate constants as a function of temperature at 1 atmospheric pressure. The total rate constant increases with increasing temperatures. At temperatures below 1000 K, the predominant contribution to the total rate constant comes from the stabilization of **1** which in turn dissociates spontaneously back to the reactants. Hence, it implies an absence of a reaction between the reactants at temperatures up to 1000 K. Between 1000 and 1500 K, the cis isomer is getting formed in addition to the redissociation of **1**. Within this temperature range, the excess energy available to the adduct **1** is not sufficient to cross **2/3** and so it leads to the stabilization of the cis isomer, **2**. Hence, k_2 contributes predominantly to the total rate constant over this temperature range. At temperatures above 1500 K, the formation of HCO + HCN overruns the stabilization

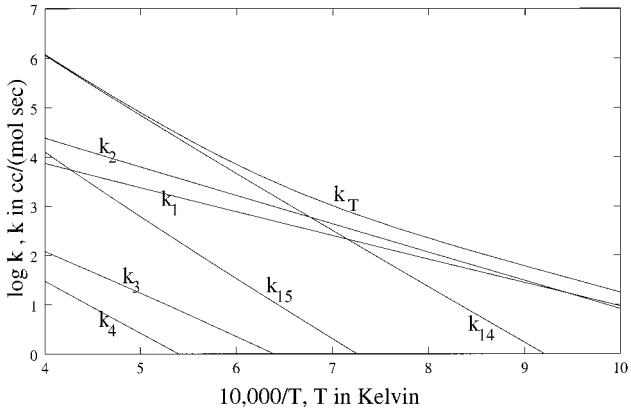

Figure 7. Plots of log apparent rate constants of the C_2H_2 + NO system vs $10^4/T$ (K) at 1 atm.

of isomers and becomes the main channel. With increase of temperature, k_{14} and in turn k_T continue to increase. Therefore, we believe that during the low-temperature pyrolysis of acetylene in the presence of NO, the radical initiation step is not caused by the NO radical. The NO radical inhibits the pyrolysis of acetylene at low temperatures by reacting with the chain carriers C_4H_3 generated from the initiation step, $2C_2H_2 \rightarrow C_4H_3 + H$. However, at higher temperatures this reaction could be the radical producing reaction as suggested by Benson.[9] The NO radical could terminate the chain polymerization by reacting with the vinyl radical produced in the reaction of H·

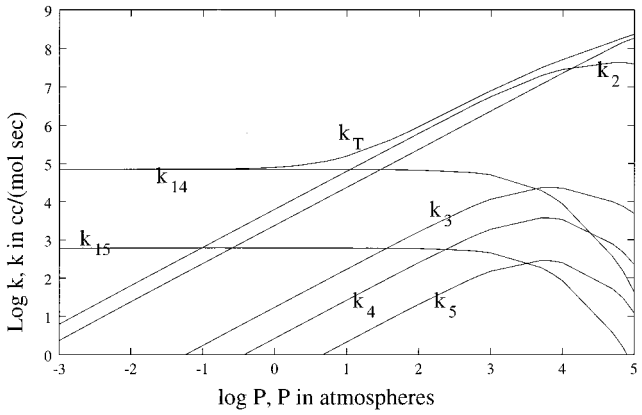

Figure 8. Plots of log apparent rate constants of the C_2H_2 + NO system versus log pressure at 2000 K.

with acetylene and thereby could lead to the adduct C_2H_3NO or its dissociation products H_2CO and HCN.

Figure 8 shows the variation of the apparent rate constants of all channels as a function of the total pressure at 2000 K. The rate of formation of adducts, (k_1, k_2, k_3, k_4, and k_5) increases with increasing pressures until 10^3 atmosphere. The total rate constant remains almost a constant until 10 atm, and the main contribution to the total rate constant k_T in the range of 0.001 to 10 atm is the k_{14} channel leading to dissociated products. At pressures beyond 10 atm, the probability for unimolecular dissociation reaction is less and the adduct **1** gets stabilized. The C_2H_2 + NO reaction has been found to be a slow reaction and at low temperatures and low pressures the system reverts back to the reactants, thereby implying an absence of a reaction. At high temperatures and low pressures, C_2H_2 + NO → HCO + HCN is the dominant reaction.

Conclusion

Both the electronic structure and rate theory calculations have been used to study the reaction between acetylene and nitric oxide on the doublet PES. While geometries and vibrational frequencies for stationary points on the potential energy surface are determined with the UB3LYP level of theory using the 6-311++G(d,p) basis set, relative energies are obtained using the larger 6-311++G(3df,2p) basis. On the doublet PES, five intermediates were found to be involved in the formation of the most favorable dissociation product, HCO + HCN. Isomerization barrier (**2** → **3**) controls the formation of HCO + HCN products and hence becomes the rate determining step in the mechanism of HCN formation. The reaction has been found to be a slow reaction, and, at low temperatures and low pressures, the system reverts back to reactants, thereby implying an absence of a reaction. Our calculated total rate constant is 7.94×10^4 cm^3 mol^{-1} s^{-1} at 2000 K and 1 atm. Our study suggests that in the pyrolysis of acetylene at temperatures below 1000 K, NO radical is not involved in the radical initiation step and it inhibits the pyrolysis by reacting with the chain carriers formed from acetylene.

Acknowledgment. We thank the FWO-Vlaanderen and GOA program for continuing support. H.M.T.N. and M.T.N. are grateful to the Flemish Government and the KULeuven Laboratory for Quantum Chemistry for supporting an "Inter-university Program for Education in Computational Chemistry in Vietnam". R.S. thanks Alexander von Humboldt Stiftung for financial support.

References and Notes

(1) Frank-Kamenetsky, D. A. *Acta Physicochim. URSS*, **1943**, *18*, 148. Frank-Kamenetsky, D. A. *J. Phys. Chem. (Moscow)*, **1944**, *18*, 329.

(2) Silcocks, C. G. *Proc. R. Soc., London* **1957**, *242A*, 411.

(3) Benson, S. W. *Int. J. Chem. Kinet.* **1992**, *24*, 217.

(4) Palmer, H. B.; Dormish, F. L. *J. Phys. Chem.* **1964**, *68*, 1553.

(5) Cullis, C. F.; Franklin, N. H. *Proc. R. Soc., London* **1964**, *280A*, 139.

(6) Minkoff, G. J.; Newitt, D. M.; Rutledge, P. *J. Appl. Chem.* **1952**, *7*, 406.

(7) Minkoff, G. J. *Can. J. Chem.* **1958**, *36*, 131.

(8) Ogura, H. *Bull. Chem. Soc. Jpn.* **1978**, *51*, 3418.

(9) Benson, S. W. *Int. J. Chem. Kinet.* **1994**, *26*, 997.

(10) Takase, H.; Kikuchi, O. *J. Mol. Struct. (THEOCHEM)* **1994**, *112*, 41.

(11) Leroy, G.; Sana, M.; Wilante, C. *J. Mol. Struct. (THEOCHEM)* **1991**, *74*, 37.

(12) Leroy, G.; Sana, M.; Wilante, C. *J. Mol. Struct. (THEOCHEM)* **1991**, *80*, 303.

(13) Pius, K.; Chandrasekhar, J. *J. Comput. Chem.* **1990**, *90*, 41.

(14) Pasto, D. J. *J. Am. Chem. Soc.* **1988**, *110*, 8164.

(15) Jursic, B. S. *Chem. Phys. Lett.* **1999**, *299*, 334. (b) Jursic, B. S. *Chem. Phys. Lett.* **1995**, *236*, 206. (c) ibid. *J. Mol. Struct. (THEOCHEM)* **1995**, *365*, 47. (d) ibid. *J. Mol. Struct. (THEOCHEM)* **1996**, *366*, 97. (e) ibid. *J. Mol. Struct. (THEOCHEM)* **1997**, *389*, 75. (f) ibid. *J. Mol. Struct. (THEOCHEM)* **1997**, *389*, 251. (g) ibid. *J. Mol. Struct. (THEOCHEM)* **1997**, *418*, 165. (h) ibid. *J. Mol. Struct. (THEOCHEM)* **1997**, *391*, 75. (i) ibid. *J. Mol. Struct. (THEOCHEM)* **1997**, *417*, 99. (j) Jursic, B. S.; Martin, R. *Int. J. Quantum Chem.* **1996**, *59*, 495. (k) Jursic, B. S.; Timberlake, J. W.; Engel, P. S. *Tetrahedron Lett.* **1996**, *37*, 97. (l) Jursic, B. S. *J. Mol. Struct. (THEOCHEM)* **1996**, *366*, 103. (m) ibid. *J. Mol. Struct. (THEOCHEM)* **1996**, *370*, 65. (n) ibid. *Int. J. Quantum Chem.* **1997**, *62*, 291. (o) ibid. *J. Mol. Struct. (THEOCHEM)* **1998**, *422*, 253. (p) ibid. *Recent Developments and Applications of Modern Density Functional Theory*; Seminario, J. H., Ed.; Elsevier: Amsterdam, 1996, p 709.

(16) Dean, A. M. *J. Phys. Chem.* **1985**, *89*, 4600.

(17) Sengupta, D.; Chandra, A. K. *J. Chem. Phys.* **1994**, *101*, 3906.

(18) Nguyen, M. T.; Sengupta, D.; Vanquickenborne, L. G. *Chem. Phys. Lett.* **1995**, *240*, 513.

(19) Nguyen, M. T.; Sengupta, D.; Raspoet, G.; Vanquickenborne, L. G. *J. Phys. Chem.* **1995**, *99*, 11883.

(20) Nguyen, M. T.; Sengupta, D.; Verecken, L.; Peeter, J.; Vanquickenborne, L. G. *J. Phys. Chem.* **1996**, *100*, 1615.

(21) Nguyen, M. T.; Sengupta, D.; Vanquickenborne, L. G. *J. Phys. Chem.* **1996**, *100*, 10956.

(22) Sengupta, D.; Nguyen, M. T. *Mol. Phys.* **1996**, *89*, 1567.

(23) Sengupta, D.; Nguyen, M. T. *Chem. Phys. Lett.* **1997**, *265*, 35.

(24) Sumathi, R.; Peyerimhoff, S. D. *Chem. Phys. Lett.* **1996**, *263*, 742.

(25) Sumathi, R.; Peyerimhoff, S. D. *J. Chem. Phys.* **1998**, *108*, 5510.

(26) Nguyen, M. T.; Sumathi, R.; Sengupta, D.; Peeters, J. *Chem. Phys.* **1998**, *230*, 1.

(27) Sumathi, R.; Sengupta, D.; Nguyen, M. T. *J. Phys. Chem.* **1998**, *102*, 3175.

(28) Sumathi, R.; Nguyen, M. T. *J. Phys. Chem. A* **1998**, *102*, 8013.

(29) Gaussian 94 Frisch, M. J.; Trucks, G. W.; Gordon, M. H.; Gill, P. M. W.; Wong, M. W.; Foresman, J. B.; Johnson, B. G.; Schlegel, H. B.; Robb, M. A.; Replogle, E. S.; Gomperts, R.; Andres, J. L.; Raghavachari, K.; Binkley, J. S.; Gonzalez, C.; Martin, R. J.; Fox, D. J.; Defrees, B. J.; Baker, J.; Stewart, J. J. P., Pople, J. A. Gaussian Inc.: Pittsburgh, PA, 1994.

(30) Baker, J.; Scheiner, A. C.; Andzelm, J. J. *Chem. Phys. Lett.* **1993**, *216*, 380.

(31) Becke, A. D. *J. Chem. Phys.* **1993**, *98*, 5648.

(32) Lee, C.; Yang, W.; Parr, R. G. *Phys. Rev. B* **1988**, *37*, 785.

(33) Baker, J.; Muir, M.; Andzelm, J. *J. Chem. Phys.* **1995**, *102*, 2065.

(34) Qin, Y.; Wheeler, A. *J. Chem. Phys.* **1995**, *102*, 1689.

(35) Barone, V. *J. Chem. Phys.* **1994**, *101*, 10666.

(36) Dean, A. M.; Westmoreland, P. R. *Int. J. Chem. Kinet.* **1987**, *19*, 207.

(37) Fan, L.; Ziegler, T. *J. Chem. Phys.* **1990**, *92*, 3645. Stanton, R. V.; Merz, K. M., Jr. *J. Chem. Phys.* **1994**, *100*, 434. Baker, J.; Andzelm, J.; Muir, M.; Taylor, P. R. *Chem. Phys. Lett.* **1995**, *237*, 53. Baker, J.; Muir, M.; Andzelm, J. *J. Chem. Phys.* **1995**, *102*, 2063. Nguyen, M. T.; Creve, S.; Vanquickenborne, L. G.; *J. Phys. Chem.* **1996**, *100*, 18422. Margl, P.; Ziegler, T.; Blöchl, P. E. *J. Am. Chem. Soc.* **1995**, *117*, 12625. Torrent, M.; Deng, L.; Duran, M.; Sola, M.; Ziegler, T. *Organometallics* **1997**, *16*, 13. Deng, Q.; Thomas, B. E., IV.; Houk, J. N.; Dowd, P., *J. Am. Chem. Soc.* **1997**, *119*, 6902.

(38) Weston, R. E. *Int. J. Chem. Kinet.* **1986**, *18*, 1259.

(39) Troe, J. *J. Chem. Phys.* **1977**, *66*, 4758.

(40) Troe, J. *J. Chem. Phys.* **1979**, *83*, 114.

(41) Scott, A. P.; Radom, L. *J. Phys. Chem.* **1996**, *100*, 16502.